Since January 2020 Elsevier has created a COVID-19 resource centre with free information in English and Mandarin on the novel coronavirus COVID-19. The COVID-19 resource centre is hosted on Elsevier Connect, the company's public news and information website.

Journal of Building Engineering 48 (2022) 103921

Contents lists available at ScienceDirect

Journal of Building Engineering

journal homepage: www.elsevier.com/locate/jobe

A practical approach for preventing dispersion of infection disease in naturally ventilated room

Chen Ren [a], Shi-Jie Cao [a,*], Fariborz Haghighat [b,a]

[a] School of Architecture, Southeast University, 2 Sipailou, Nanjing, 210096, China
[b] Energy and Environment Group, Department of Building, Civil and Environmental Engineering, Concordia University, Montreal, H3G 1M8, Canada

ARTICLE INFO

Keywords:
COVID-19
Natural ventilation
Classroom
Window-integrated fan
Infection risk

ABSTRACT

During the ongoing COVID-19 pandemic period, the airborne transmission of viruses has raised widespread concern as daily activities are resumed in public buildings. It is essential to develop mitigation strategies of infection disease transmission (e.g., increase of ventilation rate) in different scenarios to reduce the infection risk. For classrooms in schools, natural ventilation is generally used to provide outdoor air into rooms. However, the supply air volume depends strongly on the local conditions, e.g., window opening size and outdoor wind speed. In this study, the optimal design of classroom window openings is investigated, based on which low-cost window-integrated fans are then employed to enhance the efficiency of natural ventilation and infection disease control. Taking infected students as pollutant sources, numerical simulations are carried out to predict the pollutant concentration under various scenarios of pollutant sources and window opening modes (with/without fans), and to calculate the infection risk. It is found that by redesigning window openings, the airflow distribution performance index (ADPI) can be increased by 17% with corresponding infection likelihood decreased by 27%. The window-integrated fan has a significant effect on improving ventilation performance and prevention of infection disease transmission, leading to an ADPI of 99% and minimum infection probability of 11% for students sitting near the windows. This work can help to develop low-cost and effective mitigating measures of infection disease in classrooms by using hybrid ventilation systems.

1. Introduction

The outbreak of Coronavirus Disease 2019 (COVID-19) is still attracting worldwide attention [1]. As of August 2021, a cumulative total of 186 countries have been hit by this pandemic, which results in over 210 million confirmed cases and 4 million deaths with a mortality rate of 2.1% (https://covid.cdc.gov/covid-data-tracker/#global-counts-rates). It has been agreed that COVID-19 transmit primarily through close human-to-human contact as well as respiratory droplets [2]. Of these, smaller virus-containing droplets and particles (known as aerosols with the diameter less than 1 μm) can be suspended in the air over long distances [3]. In this context, the Centers for Disease Control and Prevention [4] and the World Health Organization [5] are calling for considerable attention to airborne transmission of COVID-19 and mitigation strategies especially in public spaces, such as restaurants, offices, movies, schools, etc.

In order to limit indoor airborne transmission, it is necessary to adopt additional layers of interventions like ***increasing air ventilation, adopting high efficiency filtration and air cleaning systems*** like germicidal ultraviolet air disinfection (UVGI), ***controlling***

* Corresponding author.
E-mail address: shijie_cao@seu.edu.cn (S.-J. Cao).

https://doi.org/10.1016/j.jobe.2021.103921
Received 27 October 2021; Received in revised form 14 December 2021; Accepted 18 December 2021
Available online 20 December 2021

the air distribution patterns within indoor space, and ***modifying heating, ventilating and air conditioning (HVAC) systems*** and their operation strategies [4,6]. In mechanically ventilated buildings, the dilution of airborne contaminants is done by increasing supply airflow rate. The effectiveness of this approach highly depends on the distribution of supply air in the room, and its ability to remove the contaminants from the breathing zone efficiently [7]. The distribution of supply air and efficient removal of contaminants depends on number of factors including the location and type of supply diffusers, airflow rate and temperature, etc. [8]. Increasing outdoor airflow rate will increase the building energy consumption and it is not sustainable [9]. Hence, series of low-cost and energy-efficient ventilation measures for removal of indoor air borne contaminants have been investigated, such as physical barrier [10], occupant-density-detection based ventilation system [11], UV + filtration [12], etc.

However, the huge challenge is how to control the dispersion of air borne contaminants in a naturally ventilated building, such as school, office building, etc., where the outdoor wind and indoor/outdoor temperature difference are the main driving for air exchange. The distribution and pattern of airflow in naturally ventilated building strongly depends on the location and size of the ventilation openings [13]. Xu et al. estimated the airborne infection risk in U.S. schools and analyzed the impacts of different intervention strategies, which illustrated the validity of increasing natural ventilation rate for reducing the infection risk [14]. Chen et al. indicated that the natural ventilation can reduce indoor pollutants originating from outdoor sources in the range of 5%–20% [15]. The wind-driven cross ventilation is considered as an efficient approach for ventilating public buildings [16]. Liu et al. investigated the significant effect of natural ventilation paths on the pollutant dispersion and airflow characteristic [17]. A maximum reduction of 50% in pollutant concentration was quantified for a cross-ventilated scenario commonly used in schools. The fallout of COVID-19 pandemic has demonstrated that the current cross-ventilation design schemes (e.g., number and area of doors and windows) of most buildings may be insufficient to provide the required ventilation rate to avoid the transmission of infection diseases [18]. Especially in public buildings (e.g., classrooms), the ventilation levels based on existing opening modes of windows and doors are apparently lower than the suggested ventilation standards towards COVID-19 [19]. Therefore, it is strongly suggested that the ventilation rate should be increased to 2 air-changes per hour with a mask when staying in a classroom for more than 2 h [20]. Therefore, on the basis of suggestions of social distancing ranged from 1 m to 2 m, optimizing the openings design of cross-ventilated rooms can help in the prevention of COVID-19 spread in public shared spaces.

It is important to note that various environmental factors (including season, rain, outdoor wind speed and pollutant concentration level) are major challenges in the design of naturally ventilated building [15]. Due to the unpredictability, uncertainties and stochastic nature of outdoor weather, it is necessary to combine some types of mechanical systems (i.e., hybrid ventilation system) to maintain optimal air exchange rate [21]. According to the guidance for building operations published by the American Society of Heating Refrigerating and Air-conditioning Engineers (ASHRAE) [22], the use of fans is regarded as effective strategy. Omrani et al. reviewed the vital effect of hybrid ventilation by integrating natural ventilation and ceiling fan under different scenarios on indoor air quality during pandemics [23]. The indoor air distribution is greatly influenced by the fan location and speed and the room layout [24]. conducted the air speed measurements in various commercial buildings with different room configurations, fan types and locations, and reported that the diagonal layout of ceiling fans can increase the average air velocity and uniformity. While in the case of cross-ventilation rooms (e.g., classrooms), adding fan in the window (known as window-integrated fan) is prioritized among the various schemes [4]. This approach guarantees the minimum required outdoor airflow rate and air distribution within a room. In addition, the required air distribution can be achieved by adjusting the fan speed even when the windows are closed. However,

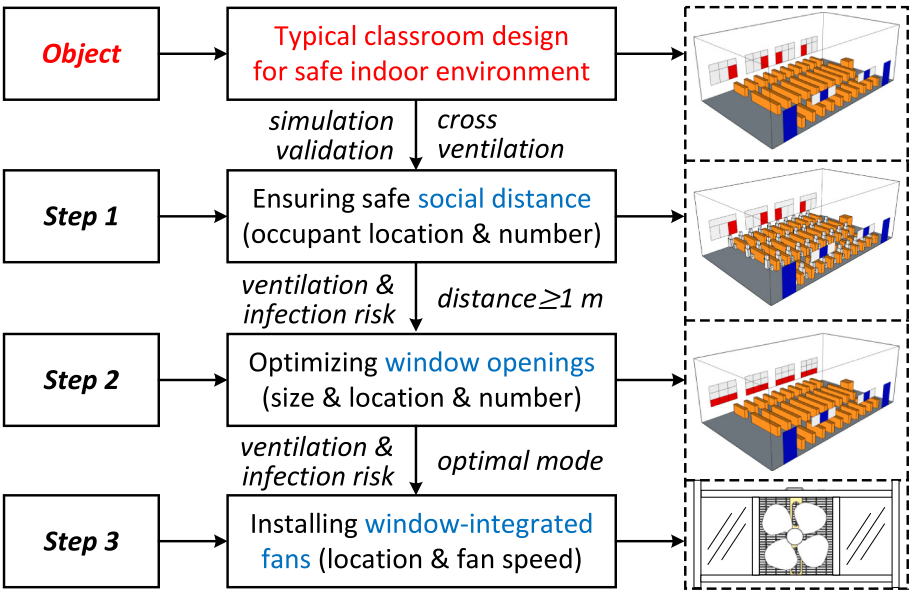

Fig. 1. Flowchart of this work aimed at typical cross-ventilated classroom design for safe indoor environment, including ensuring safe social distance, optimizing window openings and installing window-integrated fans.

systematic research is needed to comprehensively study the air distribution in a naturally ventilated classroom, and to investigate the influence of window size, location and number on the mitigating transmission of infectious diseases. A numerical simulation approach is utilized to predict the airflow and pollutant concentration distributions under different infected sources and modes. The indicators of ventilation efficiency and infection risk are used to evaluate the overall performance of various window opening modes and use of fans. The outcome of study can be used as the best practice by designers for improving the airflow distribution in a naturally ventilated room and prevention of air borne disease.

2. Materials and methods

A comprehensive numerical work is carried out to study the airflow and airborne distribution in a naturally ventilated room, where wind driven outdoor air enters the room through window opening. The flowchart of this work is shown in Fig. 1. First, experiments are performed to compare the measured data for model validation. The results of numerical simulation and grid independence are validated respectively based on the computational domains using indoor boundary and outdoor boundary. Through ensuring a safe social distance in the classroom (i.e., at least 1 m), the location and maximum number of occupants are determined. Then, the size, location and number of openings are redesigned for an optimal mode by considering ventilation efficiency and infection probability. The impacts of window-integrated fans are investigated and discussed.

2.1. Classroom model

In this study, a naturally ventilated classroom was selected. The class room is located on the 2nd floor of a university building in Nanjing [25], as displayed in Fig. 2. The classroom is 14.0 m (X) × 8.5 m (Y) × 5.0 m (Z) with a volume of 595 m^3, and it is cross-ventilated through opening doors and windows on the opposite side. There are 2 doors and 6 windows (a maximum of 2 openings) used for ventilation on the corridor side of the classroom, and 4 push-pull windows for ventilation and 4 sealed windows for daylighting on the exterior wall side. A push-pull window is consisted of fixed area and movable area (i.e., movable window), and one movable window can be opened at a time, i.e., a maximum of 4 openings for 12 push-pull windows. The dimensions of north and south window used for ventilation are 0.8 m (X) × 0.7 m (Z), and 0.8 m (X) × 1.1 m (Z), respectively. The size of south fixed window for daylighting is 2.4 m (X) × 0.55 m (Z). The door is assumed to be 1.1 m (X) × 2.1 m (Z). The classroom is set up with a front platform and 10 rows of desks, which can accommodate a maximum of 71 occupants (including 70 students and 1 lecturer) with each row of desk can accommodate 7 students. The desks on both sides of the classroom are measured as 0.30 m (X) × 1.55 m (Y) × 0.75 m (Z), and the middle desks are 0.30 m (X) × 3.10 m (Y) × 0.75 m (Z). Moreover, the distance between each row of desks is 1 m (i.e., minimum safe distance).

2.2. Experiment and simulation setups

2.2.1. Experimental monitoring

The experimental data from Ref. [25] are used for model validation, including outdoor meteorological parameters (e.g., wind speed) and indoor environmental parameters (e.g., CO_2 concentration). The experimental monitoring was performed based on a

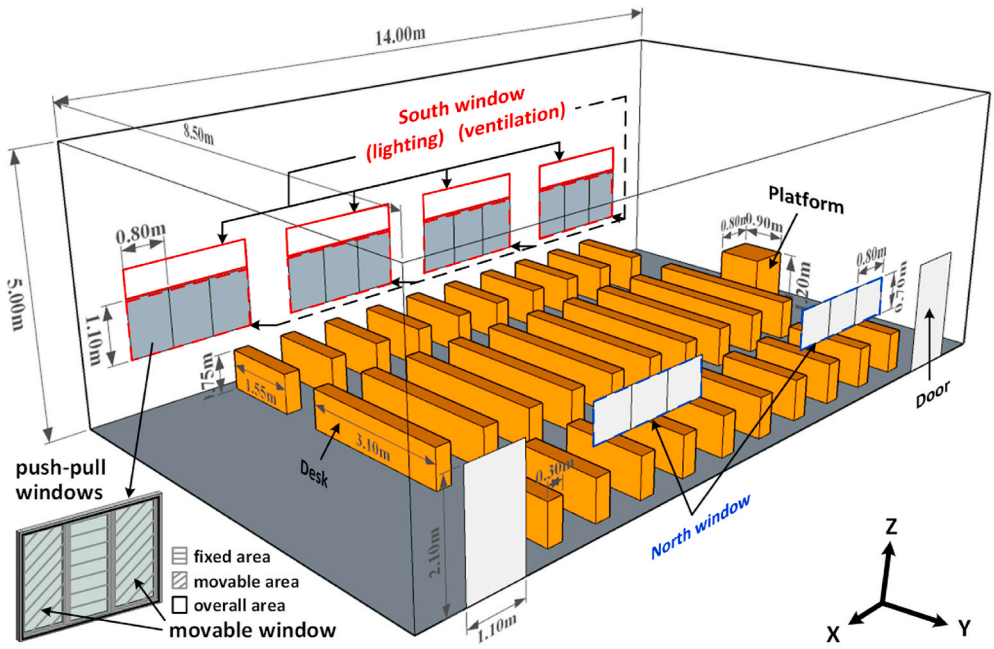

Fig. 2. Schematic diagram of a typical cross-ventilated classroom.

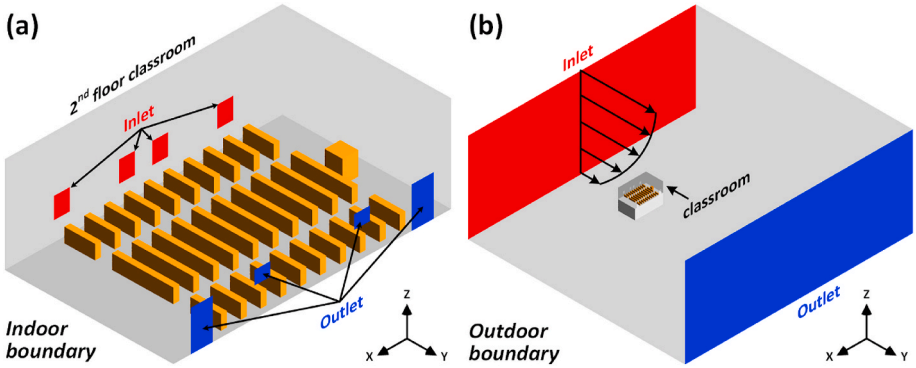

Fig. 3. Sketch maps of computational domains using (a) indoor boundary and (b) outdoor boundary for a cross-ventilated classroom with current mode.

cross-ventilated classroom from October 2012 to December 2015. The instrument utilized for outdoor wind speed monitoring was DAVIS portable weather station with the measurement range of 1–67 m/s, resolution of 0.1 m/s, and accuracy of ±5%. The experimental data were recorded at 1-min intervals. After obtaining the average CO_2 concentration in the classroom at three monitoring points, the corresponding values of air change rate per hour (ACH) are calculated using the CO_2 tracer gas decay method assuming the outdoor concentration remained constant during the experiment. The measured data of indoor and outdoor parameters are presented in Table 1.

2.2.2. Numerical simulation

The commercial ANSYS Fluent 16.0 software is adopted for numerical simulations in this study. Note that the simulation work about natural ventilation is generally carried out on the basis of the computational domain using outdoor boundary, which requires a larger grid number. In this regard, the feasibility of the computational domain using indoor boundary should be investigated for wind-driven natural ventilation (e.g., average velocity or pressure at the window openings based on the computational domain using outdoor boundary is employed as indoor inlet boundary condition), in order to simplify simulation geometry and reduce computational intensity. The driving force of temperature is not considered due to the potential negligible temperature difference between indoor and outdoor in the transition seasons (e.g., spring and autumn) that is more favorable to the usage of natural ventilation.

Fig. 3 shows the sketch maps of computational domains using indoor boundary and outdoor boundary, respectively. With regards to the indoor computational domain in Fig. 3 (a), two doors and six windows (i.e., two north and four south windows) are opened in the classroom, which is called, ***current mode***. Of this mode, the south windows are set as the inlets and the doors and north windows are set as the outlets. For outdoor domain in Fig. 3 (b), the inlet is at a 5H distance upstream and the outlet is at a 15H distance downstream (H is the height of second-floor of building, H = 10 m). The lateral and top boundaries are at 5H distances away from the targeted classroom on the second floor. Table 2 indicates the boundary conditions assigned to the computational domains using the outdoor boundary. The inflow profile of wind speed (U_z) follows the power-law type wind model with a power-law exponent (α) of 0.25, and reference wind speed (U_{ref}) is taken as 0.23 m/s at a height of H. The outlet is associated with the boundary condition of outflow, and top and lateral boundaries are modeled with symmetry boundary condition. The geometric roughness height for the ground is 1.3 m with a roughness height constant of 7. Table 3 displays the boundary conditions of computational domain using indoor boundary. The south windows for ventilation (indicated as red color in Fig. 3) are set as the velocity-inlet with the average velocity of 0.12 m/s, which can be obtained from the mean velocity magnitude at the window openings when using outdoor computational domain. The doors and north windows (blue color in Fig. 3) are modeled as the pressure-outlet. The wall and desk surfaces are non-slip walls.

An incompressible and steady-state Reynolds-averaged Navier-Stokes (RANS) model, Re-Normalization Group (RNG) k-ε model, is adopted for simulation of indoor environmental parameters, e.g., airflow velocity, pollutant concentration, etc. [26]. The general form of governing equations can be written as:

$$\nabla \cdot (\rho \mathbf{u}_i \varphi) = \nabla \cdot (\Gamma_\varphi \nabla \varphi) + S_\varphi \tag{1}$$

where, ρ is density; $\mathbf{u}_i$ is velocity vector; φ represents each of three velocity components, kinetic energy of turbulence, dissipation rate of kinetic energy of turbulence, air temperature and pollutant concentration; Γ_Φ is effective diffusion coefficient; and S_Φ is source term. For the simulation of pollutant distribution (droplets or aerosols produced by an infected student), the assumption of gaseous pollutants is made in this study. According to ASHRAE [22], viruses mainly spread by means of droplets and aerosols when an infected person coughs or sneezes. Droplets will fall to the ground within a spacing less than 1 m, while aerosols behave like gas spreading to

Table 1
Measured indoor and outdoor parameters of ACH, outdoor air volume and wind speed.

The openings: 2 doors, 2 north windows and 4 south windows (ref., Fig. 3)		
ACH (h^{-1})	Outdoor air volume (m^3/h)	Average wind speed (m/s)
1.63	969.85	0.23

Table 2
Boundary conditions of computational domain using outdoor boundary.

Boundary	Type	Conditions
Inlet	velocity-inlet	$U_z = U_{ref} \cdot (z/H)^{\alpha}$
Outlet	outflow	
Ground	rough surface	roughness height of 1.3 m with a roughness height constant of 7
Top and laterals	symmetry	
Classroom	wall	non-slip wall

Table 3
Boundary conditions of computational domain using indoor boundary.

Boundary	Type	Conditions
Inlet (south windows)	velocity-inlet	0.12 m/s
Outlet (doors and north windows)	pressure-outlet	
Walls and desks	wall	non-slip wall

longer distances. In this work, a safe social distance of at least 1 m is ensured between the students. By assuming the negligible impact of pollutant diffusions on indoor velocity field, user-defined scalar (UDS) is used for the simulation of pollutant concentration. From the previous study [10], the source intensity of an infected student (with a mask) can be assumed as 0.0001 (quantum/m^3), which is further used as a reference value for pollutant concentration (C_{ref}).

The governing equations are discretized into algebraic equations by the finite volume method. The standard wall function is employed to resolve the flow close to the wall surfaces. The SIMPLE algorithm is utilized to couple pressure and velocity fields. The convection and diffusion terms are discretized by second-order schemes. The convergence of governing equations is assumed when the residuals are less than 10^{-6}. On the basis of geometric models presented in Fig. 3, the computational domains using indoor and outdoor boundaries are discretized into medium grids with 2,282,709 tetrahedral cells and 7,288,548 tetrahedral cells, respectively. The grid independence analysis is conducted by combining a coarser grid and a finer grid for two types of computational domains. The cell numbers for the coarse, medium and fine grids is separately given in Table 4. The boundary conditions are consistent with ones in Tables 2 and 3. The dimensionless airflow velocity (U/U_{max}) values at the vertical line of a validation point inside the classroom (X= 7.0 m and Y = 2.4 m) are displayed in Fig. 4, on the foundation of computational domains using indoor boundary and outdoor boundary, respectively. The results of velocity field predicted by medium and fine grids are agreeing well to each other. The average differences between the velocity magnitudes of medium grids and fine ones are approximately less than 5%. Therefore, the medium grid setting is selected for the further simulations.

2.3. Study design

Following the three steps given in Fig. 1, this study design starts with a safe indoor environment in the classroom, i.e., a safe social distance. The ***current mode*** of window openings is given from the perspective of size, location and number of openings due to the insufficient air volume, as shown in Table 1. The installation of window-integrated fans is further considered to potentially reduce the infection risk. The evaluation models used for ***current mode*** (see Fig. 3) and ***renewed modes*** (see Fig. 7) are discussed in the next section.

2.3.1. Layout of safe social distance and pollutant sources

In this cross-ventilated classroom with ***current mode*** (Fig. 3), the maximum number of occupants is 71. With a safe indoor environment as a precondition, the social distance between students should be maintained as at least 1 m which results to 40 students, as illustrated in Fig. 5. Two students are sitting at each desk in the middle and one sitting at each desk on the lateral sides. The spacing between students in the y-direction is about 2.4 m, and the distance in the x-direction is about 1 m. In Fig. 5, the manikin model for a student remains seated by assuming the total height of 1.28 m. According to ergonomics [27], the dimension of a head (including neck) is 0.20 m (length) × 0.18 m (width) × 0.30 m (height), and the mouth is 0.02 m (length) × 0.02 m (height).

The COVID-19 infected students (wearing the masks) are considered as pollutant sources, who generate virus-carrying droplets or aerosols by coughing. Fig. 6 demonstrates the locations of three single pollutant indoor sources (S1, S2 and S3), which are respectively

Table 4
Overview of simulation cases for grid independence analysis.

Case No.	Grid type	Grid number	Conditions
1	coarse grids	747,007	computational domain using indoor boundary, and boundary conditions as same as Table 3
2	medium grids	2,282,709	
3	fine grids	4,708,534	
4	coarse grids	2,659,497	computational domain using outdoor boundary, and boundary conditions as same as Table 2
5	medium grids	7,288,548	
6	fine grids	16,419,830	

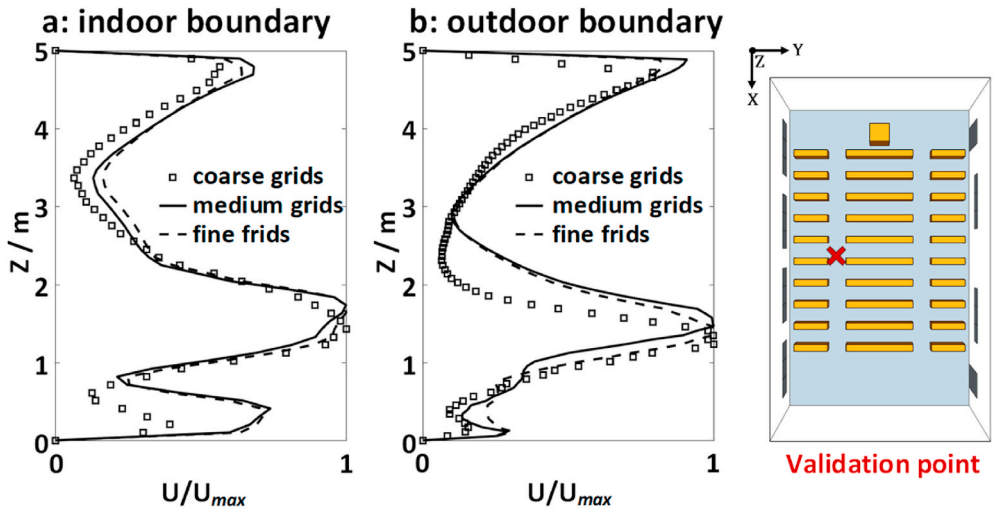

Fig. 4. Grid independence analysis for dimensionless airflow velocity (U/U_{max}) respectively based on computational domains using (a) indoor boundary and (b) outdoor boundary.

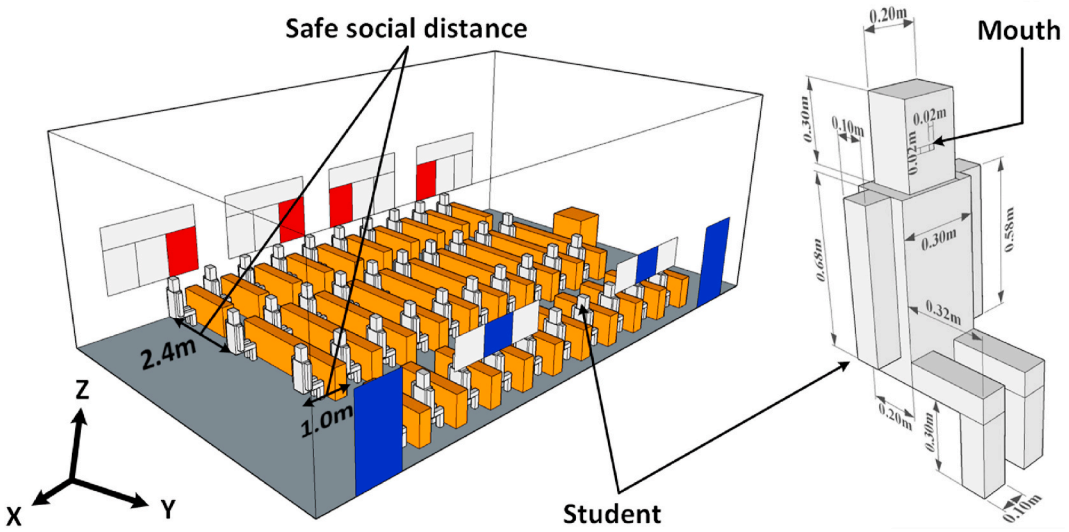

Fig. 5. Layout of indoor seated students with a safe social distance (≥1 m) in a typical classroom.

at different lines of desks with the horizontal distances of 0.69 m, 3.09 m and 7.81 m from the south wall. It is assumed that the infected student is continuously coughing with the speed of 13 m/s downwards at 27.5° [28]. The human body temperature and average breathing rate for students are respectively considered to be 36 °C and 0.7 m/s for simulations (with the area of mouth opening of 4×10^{-4} m^2). As above, the source intensity for infected student is set as 0.0001 (quantum/m^3) in the simulation. By multiplying the coughing airflow velocity and source intensity, the release quantum of pollutant per unit area (m^2) and per unit time (s) can be obtained. Based on ***current mode*** and three scenarios of pollutant sources, 4 cases (No. of 7–10) are considered for indoor ventilation performance as well as infection possibility, as shown in Table 5.

2.3.2. *Optimization of different modes of window openings*

As can be seen from Table 1, the outdoor air volume under ***current mode*** (i.e., 969.85 m^3/h) is not enough for minimum ventilation requirement in a typical classroom, which should be corresponding to 30 m^3/h per student or above [20,29]. Thus, the size, location and number of existing windows for ventilation are need to be modified, without any change to the locations of doors and north windows (see Fig. 2). A minimum of 1200 m^3/h airflow rate is needed to provide a safe indoor environment for 40 students in this classroom. Then, the total window openings area for ventilation should be increased from 3.5 m^2 (0.8 m × 1.1 m × 4) to 5.2 m^2 or more (with window opening ratios about 33%), corresponding to the fact that required outdoor air volume is increased by around 1.2 times (from 969.85 m^3/h to 1200 m^3/h).

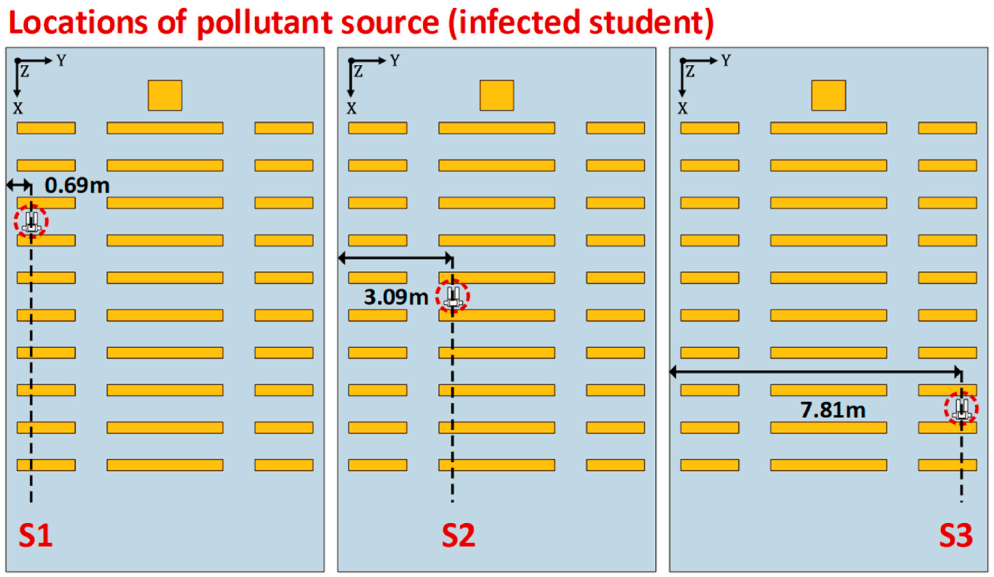

Fig. 6. Locations of three pollutant sources (infected students) of S1, S2 and S3 in a typical classroom.

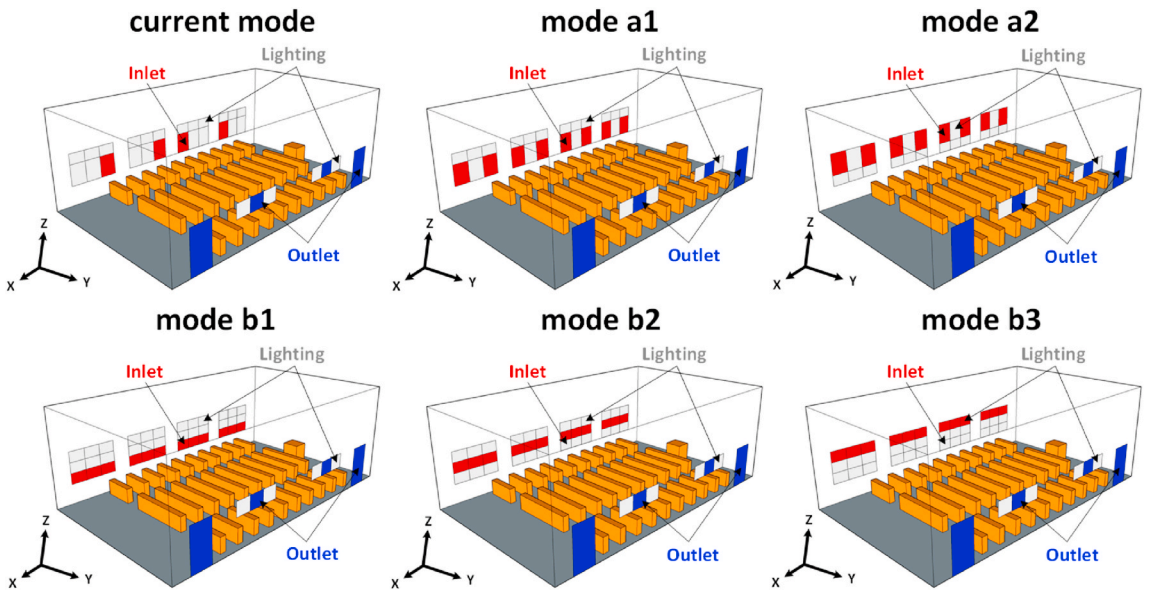

Fig. 7. Diagrams of current mode and different renewed modes of mode a1, mode a2, mode b1, mode b2 and mode b3 for window openings in a typical classroom.

Fig. 7 shows the ***current mode*** as well as ***renewed modes a1, a2, b1, b2 and b3*** for window openings in the classroom (red color for ventilation inlet and blue color for outlet). The size of a south window for ventilation in ***renewed mode a1*** and ***renewed mode a2*** is the same as ***current mode***. The number of south windows for ventilation is set as 8 under ***mode a1*** and ***mode a2***. The distances of lower edge of the south windows opening from the floor are 1 m and 1.55 m for ***renewed mode a1*** and ***mode a2***, respectively. Regarding ***renewed modes b1, b2 and b3***, the opening size for a south window is designed as 0.8 m (X) × 0.55 m (Z) and the window number is 12. For ***renewed modes b1, b2 and b3***, the heights of lower edge of south windows opening are 1 m, 1.55 m and 2.1 m, respectively. Based on five cases of ***renewed modes*** and three different scenarios based on three locations of pollutant sources, a total of 20 cases (No. of 11–30) are considered to evaluate the ventilation performance and infection risk for the optimal mode, as shown in Table 5.

2.3.3. Implementation of window-integrated fans

As depicted in Fig. 8, window-integrated fans are adopted to enhance indoor air circulation and potentially improving the removal efficiency of contaminant (virus). The number of fans is 4 with the size of 0.5 m (length) × 0.5 m (height). In order to directly deliver air to breathing region, the fans are fixed at height of 1 m from the floor. The range of fan speed is from 0 m/s to 1.98 m/s (based on 6

Table 5
Overview of simulation cases.

Case No.	Opening modes	Auxiliary device	Pollutant sources location	Notes
7	***Current mode***	Window-no fans		Evaluation of ventilation performance
8–10	***Current mode***	Window-no fans	S1, S2 and S3	Evaluation of infection risk
11–15	***Renewed modes a1, a2, b1, b2, b3***	Window-no fans		Evaluation of ventilation performance for optimal mode
16–30	***Renewed modes a1, a2, b1, b2, b3***	Window-no fans	S1, S2 and S3	Evaluation of infection risk for optimal mode
31	Optimal mode among ***current mode*** and ***renewed modes a1, a2, b1, b2, b3***	Window-integrated fans		Evaluation of ventilation performance
32–34	Optimal mode among ***current mode*** and ***renewed modes a1, a2, b1, b2, b3***	Window-integrated fans	S1, S2 and S3	Evaluation of infection risk

measurement points by using a hot-wire anemometer of Swema 03) and a maximum speed is used [30]. The maximum power consumption is 40 W that is in the range of conventional low-cost fans. Based on optimal mode of window openings, one fan location and three scenarios of pollutant sources, four cases (No. of 31–34) are considered for a comprehensive evaluation of ventilation and infection risk, as listed in Table 5.

2.4. Evaluation models

2.4.1. Ventilation index

The Air Diffusion Performance Index (ADPI) model is utilized to evaluate the airflow distribution performance under different modes of window openings (Fig. 7). ADPI is defined as the percentage of zone (below 1.2 m) that meets the acceptable indoor velocity and temperature region determined by Effective Draft Temperature (EDT) [31],:

$$ADPI = \frac{\sum_{j=1}^{M}(P_E)_j}{\sum_{i=1}^{N}P_i} \times 100\% \tag{2}$$

where, P_i is measuring point in the occupied area ($i = 1, 2, \ldots N$, and N is total number of P_i); and P_E is measuring point falling into the acceptable velocity and temperature region by calculating the EDT value ($j = 1, 2, \ldots M$, and M is the number of P_E). The EDT (^{o}C) can be written as follows [31].

$$EDT(i) = (t_i - t_a) - 8.0(v_i - 0.15) \tag{3}$$

where, t_i (^{o}C) is air temperature at the measuring point of i; t_a (^{o}C) is average air temperature in the occupied region; and v_i (m/s) is local air velocity. Since the temperature factor is not considered in this study, the value of $(t_i - t_a)$ in equation (3) can be assumed to be zero, i.e., the temperature distribution approximately achieves uniformity. Then, equation (3) can be rewritten as follows.

$$EDT(i) = -8.0(v_i - 0.15) \tag{4}$$

The criterion range of EDT is between −1.7 °C and 1.1 °C with velocity less than or equal to 0.35 m/s [32]. With the lower limit of EDT (i.e., −1.7 °C), 80% of occupants can feel comfortable according to Houghten's data [33]. Thus, ventilation performance is generally accepted when ADPI value is greater than 80%.

2.4.2. Infection risk

In order to discuss the infection risk among students under different modes of window openings and scenarios of pollutant source locations, an evaluation model of infection risk based on Wells-Riley equation is employed [34]:

$$R = \left(1 - exp\left(-IR * \int_0^T C(t)dt\right)\right) * 100\% \tag{5}$$

where, R represents infection risk (%); IR is inhalation rate of exposed student (m^3/h); t is time (h); T is total exposure time (h); and $C(t)$

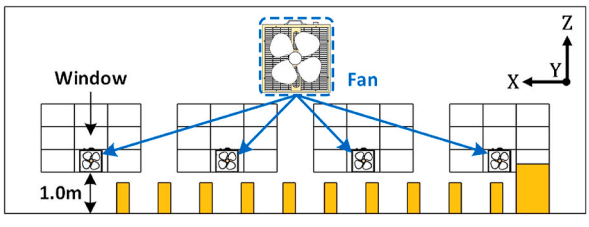

Fig. 8. Location of window-integrated fans (number is 4) in a typical classroom.

represents pollutant concentration (quantum/m^3). The *IR* value is defined as 0.96 (m^3/h) for indoor students [34], and the total exposure time is set as 1 h for the assessment of infection risk.

3. Results

In this section, indoor distribution pattern and infection likelihood are analyzed under different modes of window openings and locations of infected students in the classroom. First, based on the computational domains using indoor boundary and outdoor boundary, the simulation results of air velocity field are compared. The simulation results are also validated by the experiments. Then, the ADPI values and infection risks for various pollutant sources for ***current mode*** and five ***renewed modes*** scenarios (see Fig. 7) are obtained and compared. Finally, further simulation are carried out to obtain ADPI and infection risk for the listed scenarios for window-integrated fan case.

3.1. Model validation

The validation of simulation results from different computational domains is carried out using indoor and outdoor boundaries, respectively. Fig. 9 displays the streamlines of air velocity field at planes of Z = 1.5 and 6.5 m, and X = 7.0 m under scenario of ***current mode***. This figure shows the distributions of indoor velocity are approximately the same for two computational domains, especially for the mainstream areas at the plane of X = 7.0 m. In some regions, the simulated results of air velocity and turbulence based on indoor boundary are not as ones from outdoor boundary. However, the averaged velocity difference for the computational domains using indoor and outdoor boundaries is regarded to be negligible. Fig. 10 also presents the air velocity at the vertical lines of various validation points (P1, P2 and P3) under scenario of ***current mode***, respectively based on the computational domains using indoor and outdoor boundaries. The coordinates (X, Y) of P1, P2 and P3 are corresponding to (3.0, 2.4) m, (7.0, 2.4) m and (7.0, 4.2) m. The curves of air velocity mostly show good agreement between indoor and outdoor boundaries apart from some areas close to the floor (at P2) and the occupied zone (at P3). The main reason could be that the variation of wind direction at the windows may have an impact on indoor velocity under outdoor boundary condition, while the direction is assumed to be constant for indoor boundary condition. The mean difference between time-averaged velocity fields of using indoor and outdoor boundaries is less than 7%. It can be concluded the computational domain using indoor boundary can guarantee an acceptable accuracy for indoor velocity distribution, as compared to the case using outdoor boundary.

Fig. 11 compares measured indoor and outdoor average velocity and ACH between experiment and simulation results on the basis of computational domains using indoor boundary and outdoor boundary. The prediction deviation of indoor average velocity between the domains respectively adopting indoor and outdoor boundaries is around 4%, further proving the validity of indoor boundary. The difference of outdoor air average velocity (at the location close to the 2nd-floor classroom at a height of 10 m) between experiments and simulation results (using outdoor boundary) is less than 5%. Compared to the experimental data, the deviations of ACH acquired from the simulation using outdoor and indoor boundaries are about 2% and 7%, respectively. Hence, the reliability of numerical simulation method is well verified especially for utilizing indoor boundary to study the impact of different opening modes on the airflow distribution and infection risk.

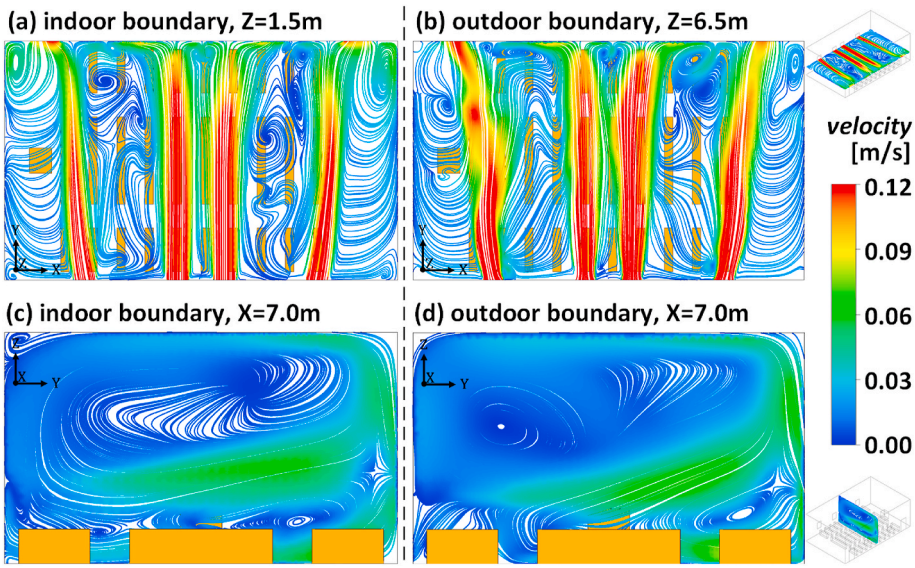

Fig. 9. Streamlines of air velocity in cross-ventilated classroom under current mode of window openings: (a) plane of Z = 1.5 m with computational domain using indoor boundary, (b) plane of Z = 6.5 m with computational domain using outdoor boundary, (c) plane of X = 7.0 m with computational domain using indoor boundary, and (d) plane of X = 7.0 m with computational domain using outdoor boundary.

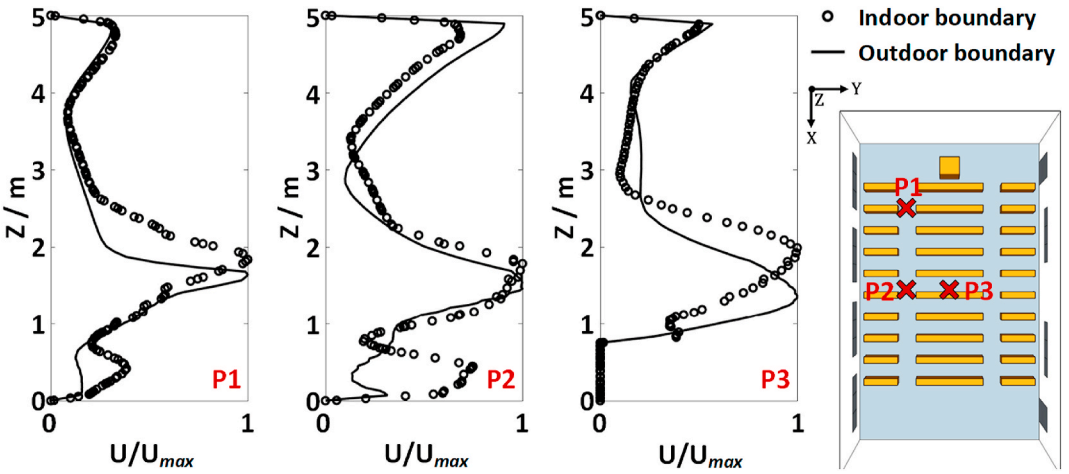

Fig. 10. Comparisons of air velocity obtained from the computational domains using indoor boundary and outdoor boundary at the vertical lines of three validation points of P1: (X, Y) = (3.0, 2.4) m, P2: (X, Y) = (7.0, 2.4) m and P3: (X, Y) = (7.0, 4.2) m in cross-ventilated classroom with current mode of window openings.

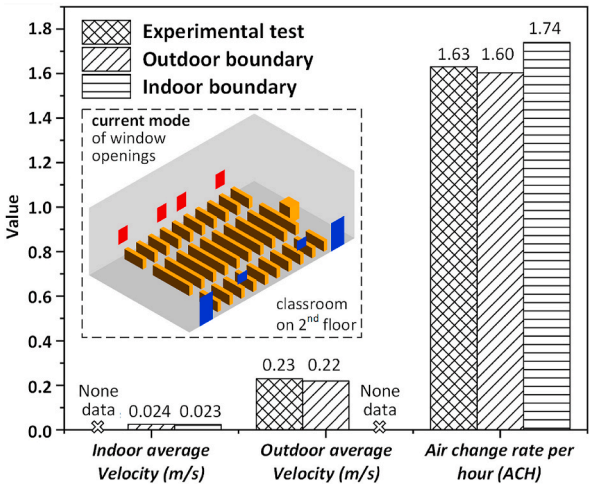

Fig. 11. Comparisons of indoor average velocity, outdoor average velocity and air change rate per hour (ACH) between experimental and simulation results from computational domains using indoor boundary and outdoor boundary around a cross-ventilated classroom with current mode of window openings.

3.2. Influence of different window openings scenarios on airflow distribution and infection risk

On the basis of ***current mode*** as well as various ***renewed modes*** of window openings scenarios, the airflow distribution performance is analyzed by using indoor boundary condition. Fig. 12 illustrates the streamlines of velocity field at the plane of Z = 1.1 m for ***current mode*** and ***renewed modes of a1, a2, b1, b2 and b3***. This figure shows that significant jet appears at a height of 1.1 m (i.e., breathing zone of students) for ***current mode*** and ***renewed modes a1 and b1***, a. Among these scenarios, ***renewed mode b1*** provides the largest coverage area of jets as the corresponding location of window openings is parallel to the plane of breathing region. For ***renewed modes a2, b2 and b3***, the supply airflow in the respiratory area is weakened as compared to ***renewed modes a1 and b1***. The explanation is that the height of south windows used for ventilation has increased from the floor (from 1 m to 1.55 m or above), leading to the vertical moving of the mainstream areas.

In order to quantify the ventilation performance, Fig. 13 indicates the ADPI values for ***current mode*** and ***renewed modes of a1, a2, b1, b2 and b3***, respectively. It can be seen that the ADPI values for ***renewed modes a1 and b1*** are significantly increased by 17.7% and 16.4% compared to the ***current mode***. The ADPI values for ***renewed modes a2 and b2*** are respectively about 61.9% and 58.6%, which represents a slight increase in comparison to the ***current mode*** of 52.6%. For ***renewed mode b3***, the ADPI is approximately equal to ***current mode***, indicating that the effect of this ***renewed mode*** is negligible on improving the airflow distribution performance. As described in subsection 2.4.1, the ventilation performance can be satisfactory when ADPI is equal to 80% or above. Therefore, it can be summarized that all ***renewed modes*** are insufficient to ensure safe and healthy environment for a cross-ventilated classroom with the precondition of lower outdoor wind speed. For the sake of delivering more air to classroom, the employment of additional equipment used for ventilation appears to be of great necessity.

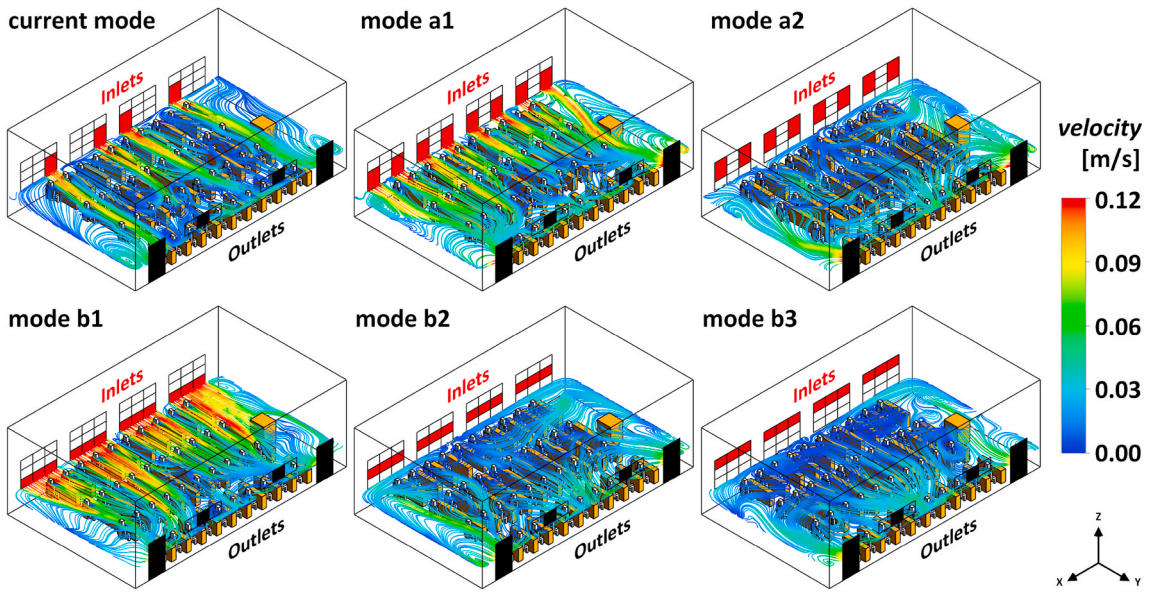

Fig. 12. Streamlines of air velocity at the plane of Z = 1.1 m between current mode and different renewed modes of mode a1, mode a2, mode b1, mode b2 and mode b3 for window openings in a cross-ventilated classroom (red color for inlets and black color for outlets). (For interpretation of the references to color in this figure legend, the reader is referred to the Web version of this article.)

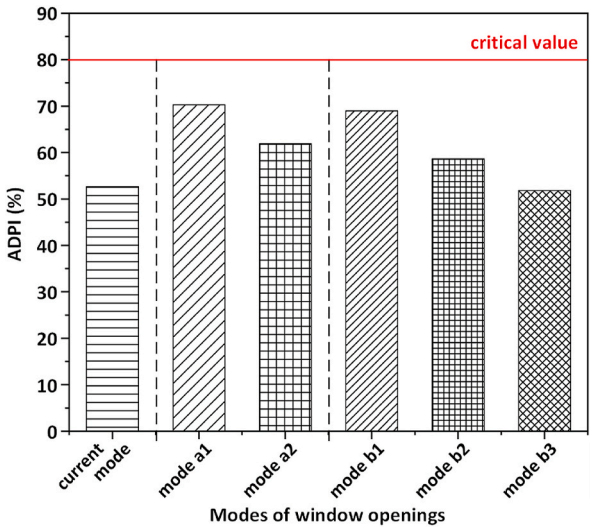

Fig. 13. ADPI values between current mode and different renewed modes of mode a1, mode a2, mode b1, mode b2 and mode b3 for window openings in a cross-ventilated classroom.

Further simulation was performed to investigate, the effect of airflow patterns under different modes of window opening on the distributions of pollutant concentration for various locations of infected source. Fig. 14 shows the relative pollutant concentration fields (C/C_{ref}), at Z = 1.1 m, for ***current mode*** and ***renewed modes a1, a2, b1, b2 and b3*** with pollutant source of S1. When the infected source is in the front area of the classroom and close to the inlets, the pollutant level in the first half of the classroom is significantly greater than one in the second half. In the ***current mode***, the pollutant concentration in the front area mostly exceeded 3%. The ***renewed modes a1, a2 and b1*** can exert better pollutant removal performance by reducing the relative concentration to less than 2% or even lower value (except for the area close to the pollutant source). The ***renewed modes b2 and b3*** are less effective in mitigating the dispersion of pollutant with the relative concentration values around 3% in some regions. In particular, the areas of concentrated contamination appear under ***renewed mode b3***, which may further exacerbate the spread of infection diseases. With the same modes as Fig. 14, the distributions of pollutant concentration at the plane of Z = 1.1 m with pollutant sources at location S2 and S3 are respectively displayed in Figs. 15 and 16. When the source is located in the center and second half of the classroom, the directions of contaminant dispersion are diversified due to the backflow (recirculation and stagnation), which may lead to increased exposure risk

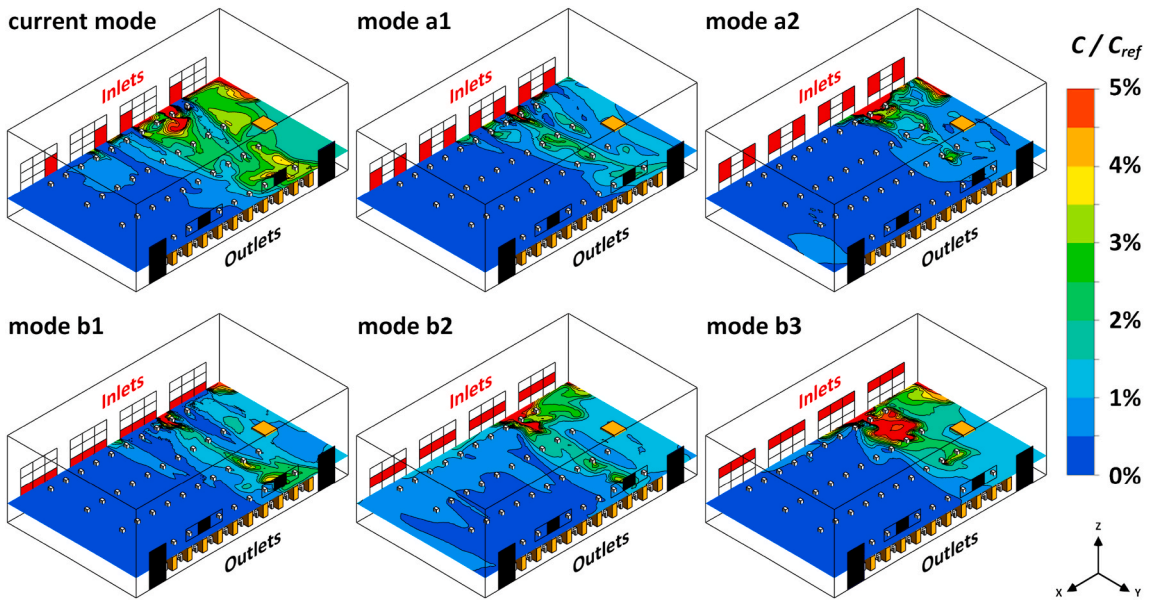

Fig. 14. Pollutant concentrations (C/C_{ref}) at the plane of Z = 1.1 m with pollutant source of S1 between current mode and different renewed modes of mode a1, mode a2, mode b1, mode b2 and mode b3 for window openings in a cross-ventilated classroom (red color for inlets and black color for outlets). (For interpretation of the references to color in this figure legend, the reader is referred to the Web version of this article.)

for students (in comparison to the infected source located at S1). With the pollutant source at S2, the total coverage of pollutant is greater than those at S1 and S3 under ***current mode***. The airflows under ***renewed modes a1 and b1*** have positive influence on lowering the pollutant concentrations. Nevertheless, ***renewed modes a2, b2 and b3*** are less efficient in the removal of contaminant. This phenomenon seems to be worse when the pollutant source is located at S3. In addition to ***renewed modes a1 and b1***, other modes can also result in accumulation of pollutants in some regions (leading the relative pollutant concentration above 5%), which can be highly detrimental (infecting more students). Besides, it should be notice that as regards ***current mode, renewed modes a1 and b1***, some airflow pattern may be remained undistributed in the plane of Z = 1.1 m due to the airflow directly traveling from inlets to outlets without mixing with indoor air. For other ***renewed modes a2, b2 and b3***, the location of inlets is away from the plane of Z = 1.1 m, resulting in weakened and less undistributed airflow at the breathing plane due to both recirculation and entrainment of indoor air. To

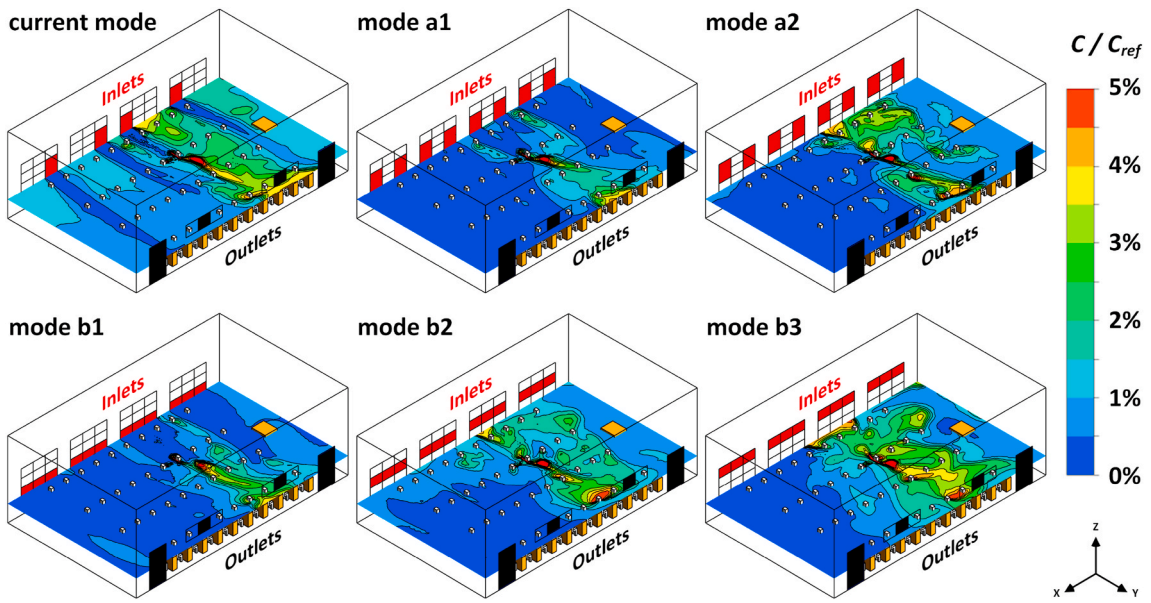

Fig. 15. Pollutant concentrations (C/C_{ref}) at the plane of Z = 1.1 m with pollutant source of S2 between current mode and different renewed modes of mode a1, mode a2, mode b1, mode b2 and mode b3 for window openings in a cross-ventilated classroom (red color for inlets and black color for outlets). (For interpretation of the references to color in this figure legend, the reader is referred to the Web version of this article.)

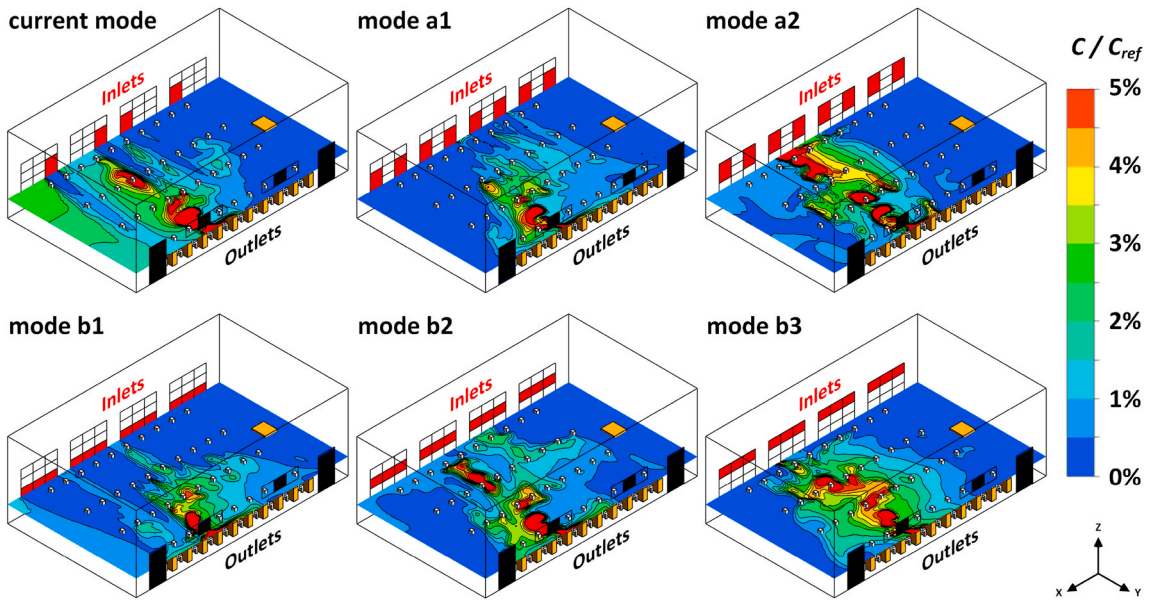

Fig. 16. Pollutant concentrations (C/C_{ref}) at the plane of Z = 1.1 m with pollutant source of S3 between current mode and different renewed modes of mode a1, mode a2, mode b1, mode b2 and mode b3 for window openings in a cross-ventilated classroom (red color for inlets and black color for outlets). (For interpretation of the references to color in this figure legend, the reader is referred to the Web version of this article.)

summarize, ***renewed modes a1 and b1*** can contribute to effective removal of pollutant rather than ***renewed modes a2, b2 and b3***.

Next, the infection probabilities under a variety of modes of window openings and locations of pollutant source are calculated utilizing the infection risk assessment model. Regarding a single source of S1, S2 and S3, the average infection risk among students is calculated (excluding the infected one). In order to estimate the infection risk in the case of coexistence of three sources, linear ventilation model (LVM) is adopted to effectively predict the pollutant concentration fields through linear superposition method. Fig. 17 depicts the infection likelihood (at exposure time of 1 h) under various scenarios based on pollutant sources of S1, S2, S3 and S1 & S2 & S3 for ***current mode*** and different ***renewed modes a1, a2, b1, b2 and b3***. For ***current mode***, the infection risk with the pollutant source at location S1, S2, S3 and S1 & S2 & S3 are 54.9%, 64.9%, 54.9% and 66.8%, respectively. Under the condition of single infected source, the maximum probability of infection occurs in the case where the location of source is S2, which should be attributed to large coverage area of pollutants. When multiple sources coexist, the indoor infection likelihood is as high as about 70%, further giving rise to an extremely serious cross-infection. For scenario ***renewed mode a1 and b1***, the average infection risk for a single source is effectively reduced with the maximum percentage of 24.6% and 26.7%, respectively. The probability of infection under three pollutant

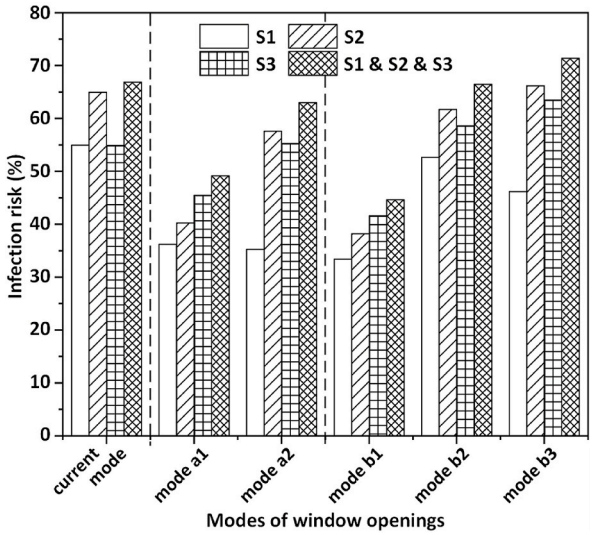

Fig. 17. Infection risk (exposure time is 1 h) with pollutant sources of S1, S2, S3 and S1 & S2 & S3 between current mode and different renewed modes of mode a1, mode a2, mode b1, mode b2 and mode b3 for window openings in a cross-ventilated classroom.

sources (S1 & S2 & S3) can also be decreased by 17.7% and 22.2%, compared to ***current mode***. With respect to ***renewed modes a2, b2 and b3***, the calculated infection probability of students is slightly changed as compared to ***current mode***, indicating that these ***renewed modes*** play negligible roles in mitigating the infection disease transmission. Besides, it can be noted that in all cases with single source, when the location is at S1, the infection risks are the lowest. The reason is that the source location is closer to window with more significant influence of the jet (from inlet to outlet), which can facilitate the discharge of more pollutants to the outlet. As the distance between source and inlet increases, the effect of the jet diminishes. Under the impact of backflow, there is a tendency for pollutant to recirculate/stagnate, which results in an increase in concentration field and infection risk. The validation of the potential impact of the spacing between infected source and window is discussed in **Supplementary A** on the variation of infection probability in a cross-ventilation classroom.

In general, the ADPI values fail to reach the expected target of 80% for ***current mode*** as well as ***renewed modes***. Nevertheless, ***renewed modes a1 and b1*** can exhibit favorable performance in improving the airflow distribution and reduction of infection risk compared to ***current mode***. Among them, the ADPI under ***renewed mode a1*** is slightly greater than that of ***renewed mode b1***, whereas the infection likelihood of ***renewed mode b1*** is lower than that of ***renewed mode a1***. Taking the infection possibility as a priority, ***renewed mode b1*** is selected as the best candidate for fans integration.

3.3. Influence of window-integrated fans on airflow distribution and infection risk

The performance of window-integrated fans is further investigated on the airflow distribution in the classroom considering ***renewed mode b1***. The installation location of fans can be referred to Fig. 8, with a maximum supply air velocity of 1.98 m/s. Fig. 18 presents the velocity streamlines at Z = 1.1 m and X = 7.0 m under ***renewed mode b1*** with window-integrated fans. Fig. 18 (b) shows the jets generated at the openings can move directly through the classroom to the outlets. The average air velocity in the breathing region (with the height of less than 1.2 m) can reach about 0.3 m/s, which is within the acceptable air velocity of 0.35 m/s that occupants can tolerate according to ASHARE Standard. However, the velocity of the mainstream area is larger than 0.5 m/s, which may increase the discomfort level and cause the potential draught risk especially when outdoor air temperature is low. The discussion on the usage situation of fans will be displayed in section 4. An ADPI of ***renewed mode b1*** with fans is calculated to be 99.7%, which is higher than the target requirement of 80% for safe and comfortable indoor environment.

It is of necessity to discuss the impact of window-integrated fans on the infection likelihood under different pollutant source location. Fig. 19 shows the pollutant concentration fields (C/C_{ref}) at the plane of Z = 1.1 m for various pollutant source location of S1, S2 and S3 for ***renewed mode b1*** integrated with fans. The values of pollutant concentration can be greatly minimized by installing fans as compared to without fans. The average concentration in the breathing zone is respectively about 0.4%, 0.6% and 0.6% for source location at S1, S2 and S3, respectively. This result indicates by adding fans to the windows can improve the air distribution and decrease the spread of airborne infection viruses.

Furthermore, Fig. 20 illustrates the infection risk (for exposure time of 1 h) for pollutant source at location S1, S2, S3 and S1 & S2 & S3 for ***current mode***, ***renewed mode b1*** without fans and ***renewed mode b1*** with fans (number is 4). In the situation of single source, the infection probability for ***renewed mode b1*** with fans can be largely reduced from 64.9% to 17.1% by 47.8% for pollutant source of S2 (compared to ***current mode***) and reduced from 41.6% to 17.1% by 24.5% for pollutant source of S3 (compared to ***renewed mode b1*** without fans). The minimal infection risk is attained as 11.1% when the pollutant source is at S1. The infection risk increases marginally to 17.1% as the infected sources are located at S2 and S3, which is due to large distance between pollutant source and window. With the number of pollutant source increases to three, the infection risk increases slightly by 3%. Thus, the implementation of window-integrated fans can be effective for the mitigation of infection diseases.

4. Discussion

The outbreak of COVID-19 pandemic has brought up the importance of designing a healthy and safe indoor environment, such as

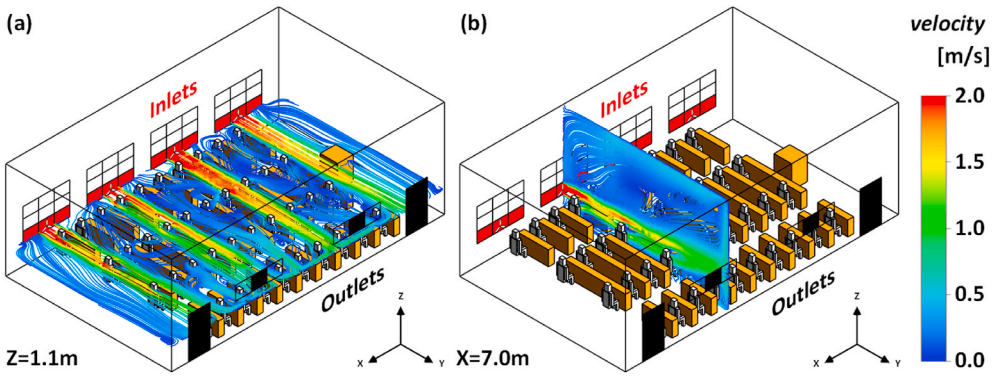

Fig. 18. Streamlines of air velocity at (a) Z= 1.1 m and (b) X = 7.0 m for renewed mode b1 with window-integrated fans (number is 4) in a cross-ventilated classroom (red color for inlets and black color for outlets). (For interpretation of the references to color in this figure legend, the reader is referred to the Web version of this article.)

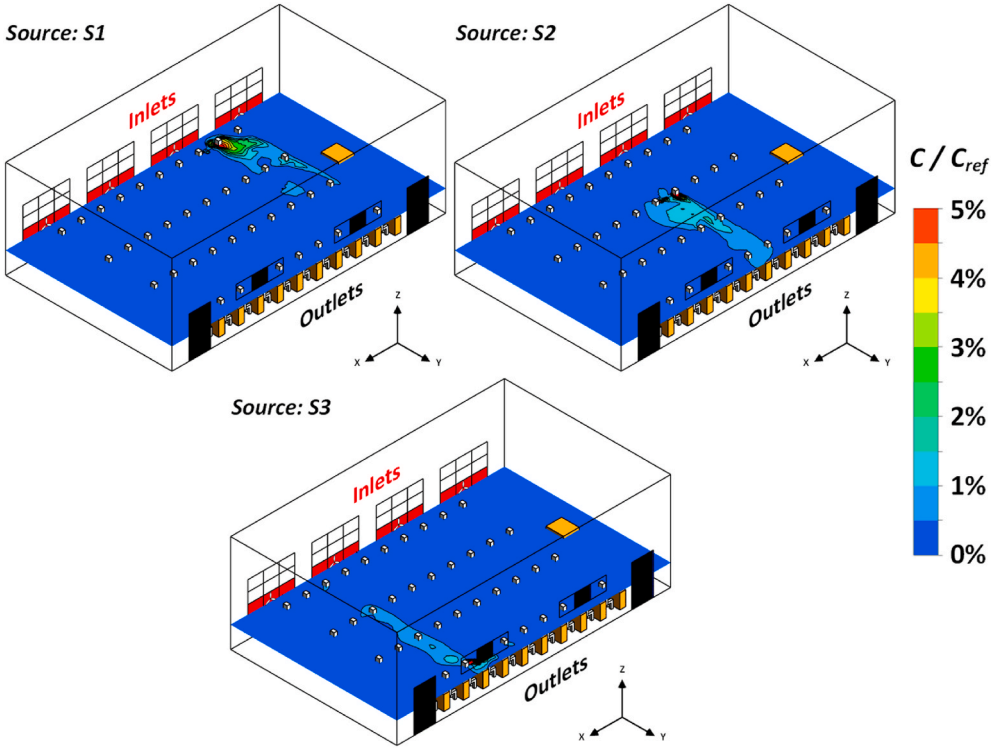

Fig. 19. Pollutant concentrations (C/C_{ref}) at the plane of Z = 1.1 m with pollutant sources of S1, S2 and S3 for renewed mode b1 with window-integrated fans (number is 4) in a cross-ventilated classroom (red color for inlets and black color for outlets). (For interpretation of the references to color in this figure legend, the reader is referred to the Web version of this article.)

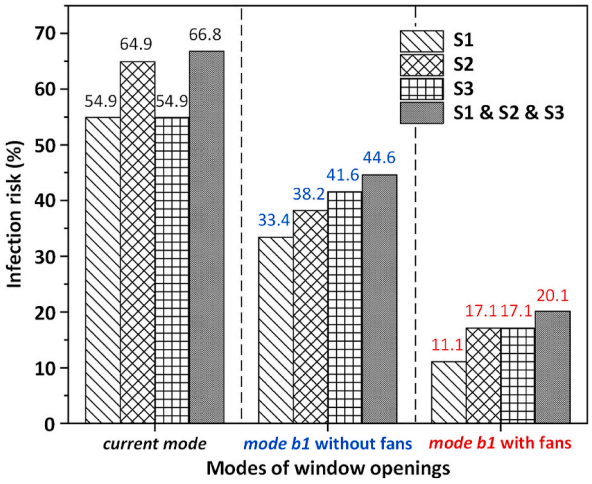

Fig. 20. Infection risk (exposure time is 1 h) with pollutant sources of S1, S2, S3 and S1 & S2 & S3 for current mode, renewed mode b1 without fans and renewed mode b1 with window-integrated fans (number is 4) in a cross-ventilated classroom.

increasing the delivery of outdoor air to dilute pollutants (viruses). This is challenging task especially in the case of naturally ventilated building where the outdoor weather is unpredictable. In this circumstance, the usage of cost-effective ventilation interventions is of great necessity, to improve air distribution performance and mitigate the spread of infection diseases. This study focuses on redesigning window opening modes (i.e., size and position) and integrating with fans. By using the optimal window openings and installing the window-integrated fans, the ventilation efficiency can be further enhanced along with the infection risk decreased.

As shown in **Supplementary B**, the mild weather conditions (such as in transitional seasons) are more favorable to the usage of fans in a naturally ventilated room, leading to the effective mitigation of infectious diseases transmission and potentially not affecting indoor thermal comfort. If the windows are closed in rainy days, the required healthy and comfortable indoor environment can be

achieved by adjusting the fan speed. However, in cold, hot or humid weather, this auxiliary ventilation measure may result in a large sacrifice in thermal comfort as well as related health risks, which is not recommended in the practical applications. In such cases, an electrical heater can be integrated with system. In occasion of highly polluted outdoor area, the system can be integrated with filtration system. A simple calculation of weather conditions (such as airflow rate, temperature, humidity and pollutant level) and draught risk may provide a guide for the usage of fans.

This study showed that a healthy and safe indoor environment can be provided in naturally ventilated room by integration of a supply fan in the window opening. The fan can be design by considering a 2.9 hr^{-1} air change as was suggested by Ref. [20]. This method is cheap and can be easily installed in almost all existing school classroom in developed and developing countries. However, the potential impact of noise from fans should also be focused on in real-life application.

The limitations of this work should be considered as well. In the simulation of pollutant concentration field, the gas contaminant is considered instead of using tracer mass and particle matter. The evaporation of liquid droplets (from large particles to small ones) is negligible as well as the impact of pollutant diffusion and heat generated by the student (air plume) on airflow distribution. For a real-life environment, more detailed setups of numerical simulation should be considered, including models and boundary conditions (such as temperature, humidity and particle pollutant). As regards poorly designed and ventilated rooms, the feasibility of low-cost prevention approaches (e.g., fans) need to be validated from the perspective of engineering application, based on the relationship of weather conditions (such as airflow rate, temperature, humidity and pollutant level) and risk (e.g., infection risk and draught risk). Regarding more types of rooms with different window openings lay out (such as single side), student numbers and spatial layouts, it is necessary to discuss the overall performance of airflow pattern and application of prevention approaches like fans (ceiling fans) [35], air purification devices [12], personalized ventilation [36], physical barriers [10] as well as additional control tools such as intelligent ventilation systems [37,38]. This can be future work.

5. Conclusions

This work investigates the impact of window designs (including optimization of window openings and implementation of window-integrated fans) on airflow distribution performance and infection risk in a naturally ventilated classroom. The ***current mode*** and various ***renewed modes*** of window openings are proposed and compared. Through installing the fans at the windows, the ventilation efficiency is further enhanced with the reduced infection risk. The results of this study can be applied in transitional seasons with conditions of mild outdoor temperature. This study can provide a reference for the design and renovation of public buildings (e.g., classrooms) using natural ventilation during the epidemic phase. The main findings are shown as follows.

(1) The numerical simulation utilizing indoor boundary can show acceptable performance for cross ventilation with the prediction errors of indoor average velocity around 4% (compared to using outdoor computational domain) and ACH value about 7% (compared to experiment).
(2) The ***current mode*** and five ***renewed modes*** of window openings fail to reach the targeted requirement of 80% for ADPI. The ***renewed mode b1*** (with 12 parallel openings at the height of 1 m from the floor) is regarded as the optimal one with ADPI increased by 16.4% and infection risk mostly reduced by 26.7% in comparison with ***current mode***. The lower infection risk is noticed when students sitting near the windows in a cross-ventilation classroom.
(3) With the implementation of window-integrated fans based on the optimal ***renewed mode b1***, the ADPI can be increased to 99.7%. Under scenario of single source and multiple sources, the infection probability can be largely decreased to about 11% and 20%, showing the effectiveness of installing low-cost fans in a cross-ventilation classroom.

Author statement

Chen Ren: Methodology, Data analysis, Writing – original draft, Writing – review & editing. Shi-Jie Cao: Supervision, Writing – review & editing Fariborz Haghighat: Conceptualization, Writing – review & editing.

Declaration of competing interest

The authors declare that they have no known competing financial interests or personal relationships that could have appeared to influence the work reported in this paper.

Acknowledgement

The authors would like to acknowledge the supports from the Natural Science Foundation of China (Grant No. 52178069 and 51778385), and Concordia University – Canada, through the Concordia Research Chair – Energy & Environment, and Postgraduate Research & Practice Innovation Program of Jiangsu Province (No. KYCX21_0112).

Appendix A. Supplementary data

Supplementary data to this article can be found online at https://doi.org/10.1016/j.jobe.2021.103921.

References

[1] F. Araya, Modeling working shifts in construction projects using an agent-based approach to minimize the spread of COVID-19, J. Build. Eng. 41 (2021), 102413.
[2] L.J. Pan, J. Wang, X.L. Wang, J.S. Ji, D. Ye, J. Shen, L. Li, H. Liu, L.B. Zhang, X.M. Shi, L. Wang, Prevention and control of coronavirus disease 2019 (COVID-19) in public places, Environ. Pollut. 292 (2021), 118273.
[3] K. Khankarl, Analysis of spread of airborne contaminants and risk of infection, ASHRAE J. 63 (2021) 14–20.
[4] CDC, Ventilation in Buildings, Centers for Disease Control and Prevention, 2021, p. 2 (June).
[5] WHO, Modes of Transmission of Virus Causing COVID-19: Implications for IPC Precaution Recommendations: Scientific Brief, World Health Organization, 2020, p. 27 (March).
[6] J.W. Ding, C.W. Yu, S.J. Cao, HVAC systems for environmental control to minimize the COVID-19 infection, Indoor Built Environ. 29 (2020) 1195–1201.
[7] C.W. Xu, X.L. Luo, C. Yu, S.J. Cao, The 2019-nCoV epidemic control strategies and future challenges of building healthy smart cities, Indoor Built Environ. 29 (2020) 639–644.
[8] Y. Lv, H.F. Wang, Y.W. Zhou, H. Yoshino, H. Yonekura, R. Takaki, G. Kurihara, The influence of ventilation mode and personnel walking behavior on distribution characteristics of indoor particles, Build. Environ. 149 (2019) 582–591.
[9] H.H. Sha, D.H. Qi, A review of high-rise ventilation for energy efficiency and safety, Sustain. Cities Soc. 54 (2020), 101971.
[10] C. Ren, C. Xi, J.Q. Wang, Z.B. Feng, F. Nasiri, S.J. Cao, F. Haghighat, Mitigating COVID-19 infection disease transmission in indoor environment using physical barriers, Sustain. Cities Soc. 74 (2021), 103175.
[11] J.Q. Wang, J.J. Huang, Z.B. Feng, S.J. Cao, F. Haghighat, Occupant-density-detection based energy efficient ventilation system: prevention of infection transmission, Energy Build. 240 (2021), 110883.
[12] Z.B. Feng, S.J. Cao, F. Haghighat, Removal of SARS-CoV-2 using UV+Filter in built environment, Sustain. Cities Soc. 74 (2021), 103226.
[13] S. Hawendi, S.A. Gao, Impact of windward inlet-opening positions on fluctuation characteristics of wind-driven natural cross ventilation in an isolated house using LES, Int. J. Vent. 17 (2017) 93–119.
[14] Y. Xu, J. Cai, S. Li, Q. He, S. Zhu, Airborne infection risks of SARS-CoV-2 in U.S. schools and impacts of different intervention strategies, Sustain. Cities Soc. 74 (2021), 103188.
[15] J.L. Chen, G.S. Brager, G. Augenbroe, X.Y. Song, Impact of outdoor air quality on the natural ventilation usage of commercial buildings in the US, Appl. Energy 235 (2019) 673–684.
[16] F. Bazdidi-Tehrani, S. Masoumi-Verki, P. Gholamalipour, Impact of opening shape on airflow and pollutant dispersion in a wind-driven cross-ventilated model building: large eddy simulation, Sustain. Cities Soc. 61 (2020), 102196.
[17] X.P. Liu, X.X. Lv, Z. Peng, C.L. Shi, Experimental study of airflow and pollutant dispersion in cross-ventilated multi-room buildings: effects of source location and ventilation path, Sustain. Cities Soc. 52 (2020), 101822.
[18] L. Morawska, J.W. Tang, W. Bahnfleth, P.M. Bluyssen, A. Boerstra, G. Buonanno, J.J. Cao, S. Dancer, A. Floto, F. Franchimon, C. Haworth, J. Hogeling, C. Isaxon, J.L. Jimenez, J. Kurnitski, Y. Li, M. Loomans, G. Marks, L.C. Marr, L. Mazzarella, A.K. Melikov, S. Miller, D.K. Milton, W. Nazaroff, P.V. Nielsen, C. Noakes, J. Peccia, X. Querol, C. Sekhar, O. Seppanen, S.I. Tanabe, R. Tellier, K.W. Tham, P. Wargocki, A. Wierzbicka, M. Yao, How can airborne transmission of COVID-19 indoors be minimised? Environ. Int. 142 (2020), 105832.
[19] S. Park, Y. Choi, D. Song, E.K. Kim, Natural ventilation strategy and related issues to prevent coronavirus disease 2019 (COVID-19) airborne transmission in a school building, Sci. Total Environ. 789 (2021), 147764.
[20] H. Dai, B. Zhao, Association of the infection probability of COVID-19 with ventilation rates in confined spaces, Build. Simulat. 13 (2020) 1321–1327.
[21] D.Y. Park, S.J. Chang, Effects of combined central air conditioning diffusers and window-integrated ventilation system on indoor air quality and thermal comfort in an office, Sustain. Cities Soc. 61 (2020), 102292.
[22] L.J. Schoen, Guidance for building operations during the COVID-19 Pandemic, ASHRAE J. 62 (2020) 72–74.
[23] S. Omrani, S. Matour, K. Bamdad, N. Izadyar, Ceiling fans as ventilation assisting devices in buildings: a critical review, Build. Environ. 201 (2021), 108010.
[24] M.H. Luo, H. Zhang, P. Raftery, L.X. Zhou, T. Parkinson, E. Arens, Y.D. He, E. Present, Detailed measured air speed distribution in four commercial buildings with ceiling fans, Build. Environ. 200 (2021), 107979.
[25] P. Liu, X.J. Xie, M. Liao, X.Y. Shen, Measured air infiltration and ventilation rates in naturally ventilated classrooms, in: Conference of ISHVAC-COBEE 2015, vol. 966, 2015, pp. 1–8.
[26] T.S. Chen, Z.B. Feng, S.J. Cao, The effect of vent inlet aspect ratio and its location on ventilation efficiency, Indoor Built Environ. 29 (2019) 180–195.
[27] E. Kahya, Mismatch between classroom furniture and anthropometric measures of university students, Int. J. Ind. Ergon. 74 (2019), 102864.
[28] H. Li, F.Y. Leong, G. Xu, C.W. Kang, K.H. Lim, B.H. Tan, C.M. Loo, Airborne dispersion of droplets during coughing: a physical model of viral transmission, Sci. Rep. 11 (2021) 4617.
[29] GB50736, Design Code for Heating Ventilation and Air Conditioning of Civil Buildings, Ministry of Housing and Urban-Rural Development, Beijing, China, 2012.
[30] R. Uday, Z.Q. Li, Y. Ke, F.M. Wang, B. Yang, Personal cooling strategies to improve thermal comfort in warm indoor environments: comparison of a conventional desk fan and air ventilation clothing, Energy Build. 174 (2018) 439–451.
[31] X. Wang, T.Q. Liu, W.L. Lee, Using revised ADPIs to identify an optimum positioning for installation of reversible room air-conditioners in bedroom for maximum thermal comfort, Build. Environ. 188 (2021), 107333.
[32] S.C. Liu, A. Novoselac, Air diffusion performance index (ADPI) of diffusers for heating mode, Build. Environ. 87 (2015) 215–223.
[33] R.G. Nevins, P.L. Miller, Analysis, evaluation and comparison of room air distribution performance-a summary, RP-55 and 88, ASHRAE (1972) (Research Report).
[34] G. Buonanno, L. Stabile, L. Morawska, Estimation of airborne viral emission: quanta emission rate of SARS-CoV-2 for infection risk assessment, Environ. Int. 141 (2020), 105794.
[35] J. Kaewrat, R.R. Janta, S. Sichum, T.C. Kanabkaew, Indoor air quality and human health risk assessment in the open-air classroom, Sustainability 13 (2021) 8302.
[36] C.W. Xu, W.B. Liu, L. Liu, S.J. Cao, Y.J. Ren, Non-uniform risk assessment methods for personalized ventilation on prevention and control of COVID-19, Chin. Sci. Bull. 66 (2021) 465–474.
[37] J.Q. Wang, C.W. Yu, S.J. Cao, Technology Pathway of Efficient and Climate-Friendly Cooling in Buildings: towards Carbon Neutrality, 30, Indoor Built Environ, 2021, pp. 1307–1311.
[38] S.J. Cao, Z.B. Feng, J.Q. Wang, C. Ren, H.C. Zhu, G. Chen, J.T. Mei, Ergonomics-oriented Operation, Maintenance and Control of Indoor Air Environment for Public Buildings, Chin. Sci. Bull., 2021, https://doi.org/10.1360/TB-2021-1024. Published Online.